IOP Publishing Semiconductor Science and Technology
Semicond. Sci. Technol. 33 (2018) 125015 (7pp) https://doi.org/10.1088/1361-6641/aae9af

Magneto-optical Kerr spectroscopy in ferromagnetic semiconductors: determination of the intrinsic complex magneto-optical Voigt constant

H Riahi[1,2], M A Maaref[3], A Lemaître[4] and Kui-juan Jin[1,2,5]

[1] Beijing National Laboratory for Condensed Matter Physics, Institute of Physics, Chinese Academy of Sciences, Beijing 100190, People's Republic of China
[2] University of Chinese Academy of Sciences, Beijing 100049, People's Republic of China
[3] Laboratoire Matériaux Molécules et Applications, IPEST, Université de Carthage, La Marsa, Tunisie
[4] Centre de Nanosciences et Nanotechnologie—CNRS, Route de Nozay, 91460 Marcoussis, France
[5] Collaborative Innovation Center of Quantum Matter, Beijing 100190, People's Republic of China

E-mail: hassen@iphy.ac.cn

Received 8 August 2018, revised 2 October 2018
Accepted for publication 19 October 2018
Published 7 November 2018

Abstract

Thin films of ferromagnetic semiconductors of the (Ga, Mn)(As, P) family are investigated by means of magneto-optical Kerr spectroscopy in order to determine the spectral dependence of the complex magneto-optical Voigt constant Q, an intrinsic parameter responsible for Kerr rotation and ellipticity. We obtain the spectral dependence of these two conjugate quantities: the Kerr rotation and ellipticity angles. Contrary to strongly absorbing metallic ferromagnetic layers, it is expected that they vary non-linearly with the layer thickness at a fixed wavelength, as a consequence of the weak absorption and the non-negligible optical phase shift in weakly absorbing semiconductor ferromagnets. We show that, from the Kerr rotation and ellipticity angles and the complex refractive index –obtained by ellipsometric measurements—we are able to determine the spectral dependence of the complex intrinsic Voigt constant, thus avoiding the need for samples with different thicknesses. Incidentally, the use of phosphorus substituted (Ga, Mn)As provides an out-of-plane magnetic easy axis, the appropriate configuration for polar magneto-optical Kerr effect, without the need for a strong external magnetic field.

Keywords: ferromagnetic semiconductors, polar Kerr effect, Voigt constant

(Some figures may appear in colour only in the online journal)

1. Introduction

The magneto-optical Kerr effect (MOKE) is a widely used technique for the investigation of the magnetic properties and the electronic structure of magnetic layers and nanostructures [1, 2] and for applications in magnetic data storage and retrieval [3, 4]. This effect consists of the rotation of the polarization plane of linearly polarized light and the appearance of ellipticity upon reflection off a magnetized material. When spatially resolved, as in MOKE microscopy, or time–resolved as in laser pump-probe experiments (TR-MOKE) it proves to be a powerful and insightful tool to investigate exciting phenomena in spintronics and magnonics such as magnetic domain wall motion [5–9], spin waves excitation and detection [10, 11] and to demonstrate novel concepts such as the optical spin transfer torque [12–14] and acoustic wave-induced magnetization switching [15, 16]. In this respect ferromagnetic diluted semiconductors (FDS) have proved to be a test-bench material owing to their easily adjustable magnetic properties [17–20].

In order to optimize the optical detection either for magneto-optical imaging or in time-resolved experiments, it

is important to determine the wavelength dependence of the MOKE. However, the MOKE is also dependent on the layer thickness, the layer and substrate indices, all the more in weakly absorbing magnetic materials as semiconductors or insulators [21–24]. It is therefore of prime importance to retrieve the intrinsic magneto-optical parameters, depending only on the bulk material structure. One such parameter is the so-called Voigt constant Q, which enters the off-diagonal components of the macroscopic dielectric permittivity tensor ε [25, 26]. For magnetization along the z-axis the dielectric permittivity tensor of an otherwise isotropic material has the following form [25]:

$$\varepsilon = \begin{pmatrix} \varepsilon_{xx} & iQ\varepsilon_{xx} & 0 \\ -iQ\varepsilon_{xx} & \varepsilon_{xx} & 0 \\ 0 & 0 & \varepsilon_{zz} \end{pmatrix}$$

where the complex parameter $Q = Q_r + iQ_i$ depends linearly on the magnetization M. For light propagation along the z-axis (polar Kerr geometry), the eigen modes are left and right circularly polarized. Their propagation with different velocities and absorption coefficients gives rise to the Faraday (in transmission) and Kerr (in reflection) effects: i.e. the linear polarization rotation and ellipticity.

Previous studies have been reported in this context. Haidu *et al* determined the dielectric function of cuprous oxide by spectroscopic ellipsometry and MOKE spectroscopy [27]. Liu *et al* obtained the off-diagonal components of the dielectric tensor of manganite perovskites based on $La_{1-x}Sr_xMnO_3$ films by analyzing Kerr rotation and ellipticity [28]. They were found that the peak position and intensity of MO spectra are very sensitive to the film thickness. Despite the increasing role of ferromagnetic semiconductors over the last two decades and the extensive studies available on their magnetic properties, there are few experimental studies of their magneto-optical properties [23, 24]. Sun *et al* studied the polar Kerr rotation for GaMnAs samples with out-of-plane magnetic easy axis and modeled the dielectric function but did not study the layer thickness dependence of the magneto-optical effects [23]. Terada *et al* measured the Kerr ellipticity spectra of (Ga, Mn)As thin films with various thicknesses [24], which enabled them to model the spectroscopic dependence of the off –diagonal element of the dielectric tensor. However, they had to use a strong magnetic field (1 T) to pull the magnetization perpendicular to the plane, which possibly gives an additional Kerr signal at the band gap of the GaAs substrate.

The aim of the present work is to extract the spectral dependence of the Voigt constant of FDS thin layers of the GaMnAs family in the visible range, in order to provide tools for optimizing the detection in MOKE microscopy and TR-MOKE experiments as well as to supply further support for future theoretical interpretation of the optical spectra. We use GaMnAs on a GaInAs substrate and phosphorus substituted GaMnAs samples in order to obtain a perpendicular-to-plane magnetic easy axis and thus avoid the need for a strong magnetic field to pull the magnetization out of the plane. A 3-layer model is used to extract the variation of the real and imaginary parts of Q from PMOKE rotation and ellipticity spectra using the film thickness and the complex refractive index, which is determined from spectroscopic ellipsometry above the Curie temperature on a similar (Ga, Mn)(As,P) layer.

2. Sample growth and experimental details

We studied three samples of $Ga_{1-x}Mn_xAs_{1-y}P_y$ layers with different concentrations of phosphorus. They were grown by low temperature molecular beam epitaxy.

The first sample consists of a 50 nm thick $(Ga_{0.93}, Mn_{0.07})As$ layer grown on a $Ga_{1-y}In_yAs$ relaxed buffer layer, itself deposited on a (GaAs) template. Details can be found in Ref [15]. The two $Ga_{1-x}Mn_xAs_{1-y}P_y$ samples (B and C) have the same thickness as sample A and they were grown on a GaAs substrate. The nominal concentrations of Mn and P were calibrated using Vegard's law, based on the lattice constants from a reference (Ga, Mn)As [(Ga, As)P] sample grown under the similar condition, a particular, a similar substrate temperature [17, 29]. For all these samples, the total Mn concentration was fixed to $x = 0.07$. The phosphorus percentage was set to $y = 0\%$, $y = 8.8\%$ and $y = 11.3\%$ for A, B and C layers, respectively. Details can be found in table 1. After the growth, they were systematically annealed under N_2 atmosphere at 250 °C for 1 h in order to improve their magnetic properties [30].

From magnetometry measurements, the Curie temperatures were found to be 125 K, 55 K and 52 K for samples A, B, and C, respectively. The active Mn concentration x_{eff} is extracted from the saturation magnetization M_s at low temperature as: $x_{eff} = M_s/N_0 g\mu_B S$ [6], where $S = 5/2$, N_0 is the density of cation sites in the lattice, g is the Landé factor taken as $g = 2$ and μ_B is the Bohr magneton.

The hysteresis loops of the three samples show a similar square shape at $T = 10$ K indicating that the magnetization easy axis is perpendicular to the layer plane. The coercitive field (H_c) for sample A is slightly lower ($H_c \sim 6$ mT) than for the B and C samples ($H_c \sim 7.4$ mT and 8.8 mT, respectively).

The MOKE measurements are performed in polar geometry in which the incident light beam was quasi-normal on the surface of the sample. Details of the experimental setup are found in [31, 32]. The sample was illuminated with a monochromatic light from a 150 W Xe lamp. Light with selected wavelength was then polarized with a Glan-Thompson polarizer. The linearly polarized light was modulated by a mechanical chopper and a photo-elastic modulator (PEM), at $f_0 = 250$ Hz and $f = 50$ kHz, respectively. The reflected beam passed through an analyzer and its intensity was detected with a Si photodiode. The detected signal was fed into two lock-in amplifiers. The first and second look-in amplifiers were referenced to the chopper (f_0) and to the PEM frequencies (f or 2f), respectively. The Kerr rotation angle θ_K and the ellipticity angle ψ_K were obtained from the signals at the PEM frequencies, 2f and f, respectively. The average reflected intensity is obtained from the signal modulated by the chopper frequency [33]. The sample temperature was

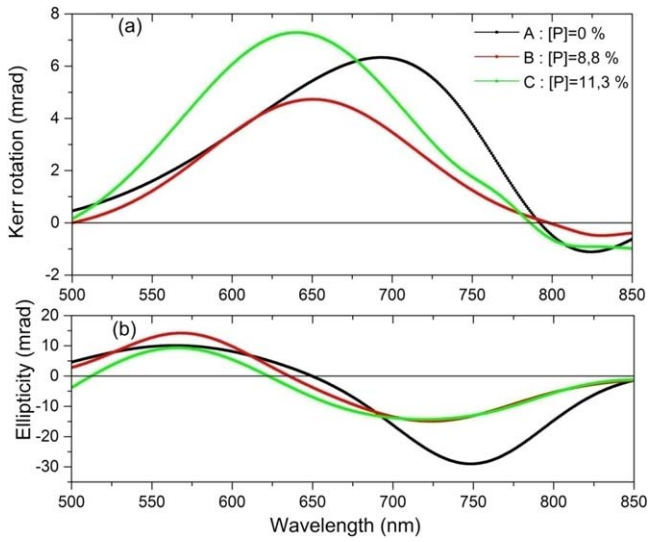

Figure 1. Kerr rotation (a) and ellipticity (b) spectra at T = 10 K for samples A, B and C.

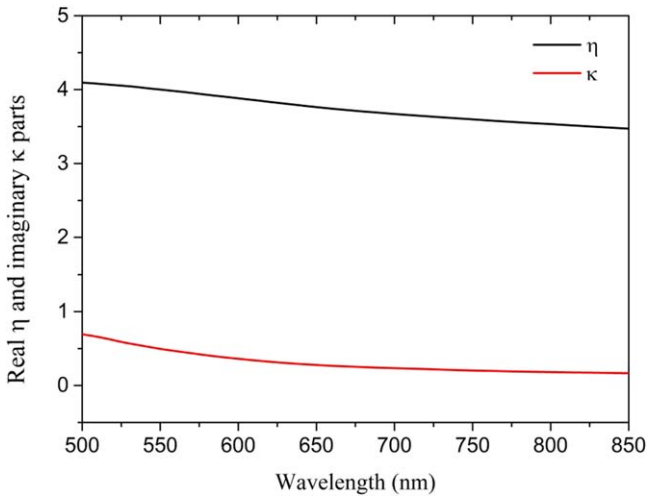

Figure 2. Spectra of the real and imaginary parts of refractive index n at room temperature.

Table 1. $Ga_{1-x}Mn_xAs_{1-y}P_y$ sample parameters: the manganese and phosphorus concentrations are denoted [Mn] and [P], respectively, the effective Mn concentration x_{eff}, the saturation magnetization M_s at T = 10 K, the Curie temperature T_C, the uniaxial strain ε_{zz} at room temperature, and the uniaxial perpendicular anisotropy constant $K_{2\perp}$ at T = 10 K.

Samples	A	B	C
[Mn] (%)	7	7	7
[P] (%)	0	8.8	11.3
x_{eff}(%)	3.7	3.5	3.4
M_s (kA m^{-1})	38.6	33	35
T_C(K)	125	55	52
ε_{zz} (%)	−0.17	−0.23	−0.33
$K_{2\perp}$(kJ m^{-3})	11.2	0.48	0.15

varied between 10 and 300 K with a closed-cycle liquid helium cryostat. Only data at T = 10 K are presented here. During the measurement, a 20 mT external magnetic field B was applied perpendicular to sample surface in order to define the magnetization direction and the PMOKE spectra where then measured for +B and –B. θ_K and ψ_K are obtained from the difference of the signals at +B and −B, respectively.

The wavelength dependence of the real η and imaginary κ parts of refractive index n are obtained from ellipsometry measurements at room temperature on a similar sample.

3. Results and discussion

Figure 1 displays the spectral dependence of the Kerr rotation and Kerr ellipticity of the A, B, and C samples at T = 10 K. Kerr rotation and ellipticity show distinct spectral features in the spectral range λ = 500 nm to 850 nm. θ_K of sample A has a considerable variation versus incident energy and it has a pronounced positive peak (about 6.5 mrad) at ∼700 nm. As compared with previous experimentally works on (Ga, Mn) As, θ_K keeps the same magnitude [33]. For sample B, the Kerr rotation reached 4.7 mrad at ∼652 nm. With increasing P concentration up to [P] = 11.3%, θ_K was enhanced to 7.3 mrad. It is clear from figure 1(a) that θ_K was blue shifted with increasing P concentration. Microscopically, the Kerr rotation originates from transitions between the valence and conduction bands. Previous theoretical works on $GaAs_{1-x}P_x$ layers has been shown that the energy-band gap (Eg) increased with increasing P doping [34]. The blue shift identified between the studied layers was also observed in theoretical and experimental previous works as a function of Mn and P doping [32, 35, 36]. Indeed, Yahyaoui *et al* highlighted the enhancement of Eg as a function of P doping in (Ga, Mn)(As, P) layers [37]. They found that the Eg increases from 1.52 eV to 1.61 eV for [P] = 7% and [P] = 11.3%, respectively. Also, Sun *et al* showed an energy band-gap around Eg = 1.5 (eV) for $Ga_{0.95}Mn_{0.05}As/GaInAs$ layer [23]. Comparing the Eg variation with θ_K peaks, one can note that the blue shift of Kerr rotation as a function of P doping is in good qualitative agreement with Eg increasing. In figure 1(b) we show the spectral variation of the Kerr ellipticity for the three samples. The magnitude of the Kerr ellipticity is larger than the magnitude of the Kerr rotation. The amplitude of the ellipticity for sample A has a considerable variation as compared with B and C samples. For sample A, ψ_K changes sign at higher wavelengths with respect to the two other samples and reaches its largest absolute value maximum, 30 mrad, at 750 nm. As a comparison between the obtained spectra, one can conclude that the Kerr rotation and Kerr ellipticity have the form of bell-shaped curve and its derivative, respectively, as usually found in the vicinity of an optical transition [33]. The asymmetry of θ_K and ψ_K peaks of sample A, as compared with B and C samples, may be due to the effect of (Ga,In)As substrate.

The wavelength dependence of refractive index n of $Ga_{0.93}Mn_{0.07}As_{0.93}P_{0.07}$ layer is shown in figure 2. The real η and imaginary κ parts of n are obtained from ellipsometry measurements at room temperature. It is clear from this figure

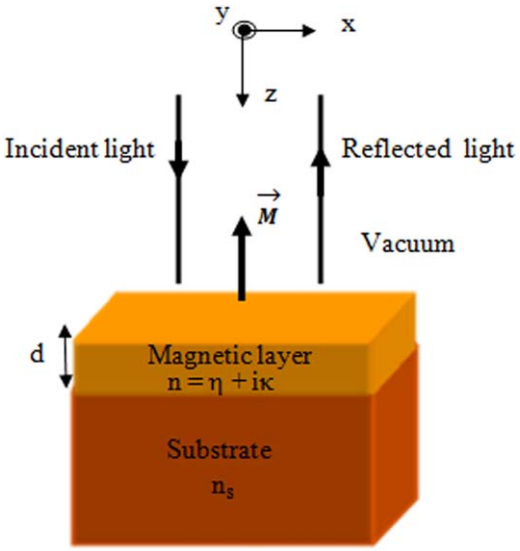

Figure 3. Schematic illustration of the 3-layer model. The incident light and the magnetic field are perpendicular to sample surface. The complex refractive index and the thickness of magnetic layer are denoted n and d, respectively.

that the magnitude of κ, which is related to the light absorption in this layer, is very small compared to that of the real part.

4. Model

In the framework of the model schematically depicted in figure 3, we discuss the analysis of the experimental data obtained from the static MOKE calculation is restricted to the case of normal incidence of light (along the z direction).

Assuming in the first approximation that the refractive index of the substrate n_s is equal to n: the static Kerr rotation θ_K and ellipticity ψ_K can be written as [22]:

$$\theta_K(\lambda) = \frac{4\pi}{\lambda}\mathrm{Re}\left(\frac{n^2 Q}{(n^2-1)}\int_0^d m_z(z)\exp\left(\frac{4i\pi nz}{\lambda}\right)dz\right) \quad (1)$$

$$\psi_K(\lambda) = \frac{4\pi}{\lambda}\mathrm{Im}\left(\frac{n^2 Q}{(n^2-1)}\int_0^d m_z(z)\exp\left(\frac{4i\pi nz}{\lambda}\right)dz\right) \quad (2)$$

Where m_z is the z-component of the unit vector of the magnetization.

In the case of a homogeneous equilibrium magnetization $m_z(z) = 1$ for materials with a high absorption coefficient ($\alpha \gg 1/d$) such as manganite perovskytes [38] or for a magnetic layer much thicker than the absorption length, the Kerr rotation and ellipticity take the form calculated for a semi-infinite magnetic medium [2]: $\theta_K^\infty = \mathrm{Im}\left[\frac{n\ Q}{n^2-1}\right]$, $\psi_K^\infty = -\mathrm{Re}\left[\frac{n\ Q}{n^2-1}\right]$. Furthermore, in the latter case, if absorption is weak ($\kappa \ll \eta$), these two parameters have the following form [1, 2]:

$$\theta_K^\infty(\lambda) = \frac{\eta\,(\eta^2-1)\,Q_i - \kappa(\eta^2+1)\,Q_r}{(\eta^2-1)^2} \quad (3)$$

$$\psi_K^\infty(\lambda) = -\frac{\kappa(\eta^2+1)\,Q_i + \eta\,(\eta^2-1)Q_r}{(\eta^2-1)^2} \quad (4)$$

In FDS, the Kerr rotation and ellipticity vary non-linearly with the film thickness. They depend on the thickness of the film with respect to the absorption length $1/\alpha$ with α the absorption coefficient $\alpha = \frac{4\pi\ \kappa}{\lambda}$ and they are modulated by the optical phase $\phi_{opt}(\lambda) = \frac{4\pi\ \eta\ d}{\lambda}$. In the limit of weak absorption, one obtains:

$$\theta_K(\lambda) = \theta_K^\infty(\lambda) + \exp(-\alpha d) \times (\psi_K^\infty(\lambda)\sin(\phi_{opt}) - \theta_K^\infty(\lambda)\cos(\phi_{opt})) \quad (5)$$

$$\psi_K(\lambda) = \Psi_K^\infty(\lambda) - \exp(-\alpha\ d) \times (\theta_K^\infty(\lambda)\sin(\phi_{opt}) + \psi_K^\infty(\lambda)\cos(\phi_{opt})) \quad (6)$$

We notice the appearance of two oscillating terms in the two equations (5) and (6), which depends on the ratio of the layer thickness to the wavelength of the light in the magnetic layer $d\eta/\lambda$. It is worth nothing that these additional terms mix the Kerr rotation and ellipticity coefficients of the infinite material. They can lead to strong enhancement or cancellation of the Kerr rotation or ellipticity for a specific thickness or wavelength. From equations (5) and (6) we extract the two expressions related to the Kerr rotation and ellipticity for an infinite thickness of magnetic layer as:

$$\theta_K^\infty(\lambda) = \frac{\psi_{K\exp}(\lambda)\sin(\phi_{opt}) + \theta_{K\exp}(\lambda)(\cos(\phi_{opt}) - \sinh(\alpha\ d) - \cosh(\alpha\ d))}{2(\cos(\phi_{opt}) - \cosh(\alpha\ d))} \quad (7)$$

$$\psi_K^\infty(\lambda) = \frac{\psi_{K\exp}(\lambda)(\cos(\phi_{opt}) - \sinh(\alpha\ d) - \cosh(\alpha\ d)) - \theta_{K\exp}(\lambda)\sin(\phi_{opt})}{2(\cos(\phi_{opt}) - \cosh(\alpha\ d))} \quad (8)$$

Figure 4 shows the expected Kerr rotation and ellipticity spectra expected for an infinite thickness of samples A, B and C, obtained from equations (7) and (8). By comparing this figure with the experimental data in figure 1, one can note that the changes with respect to the infinite layer are clearly

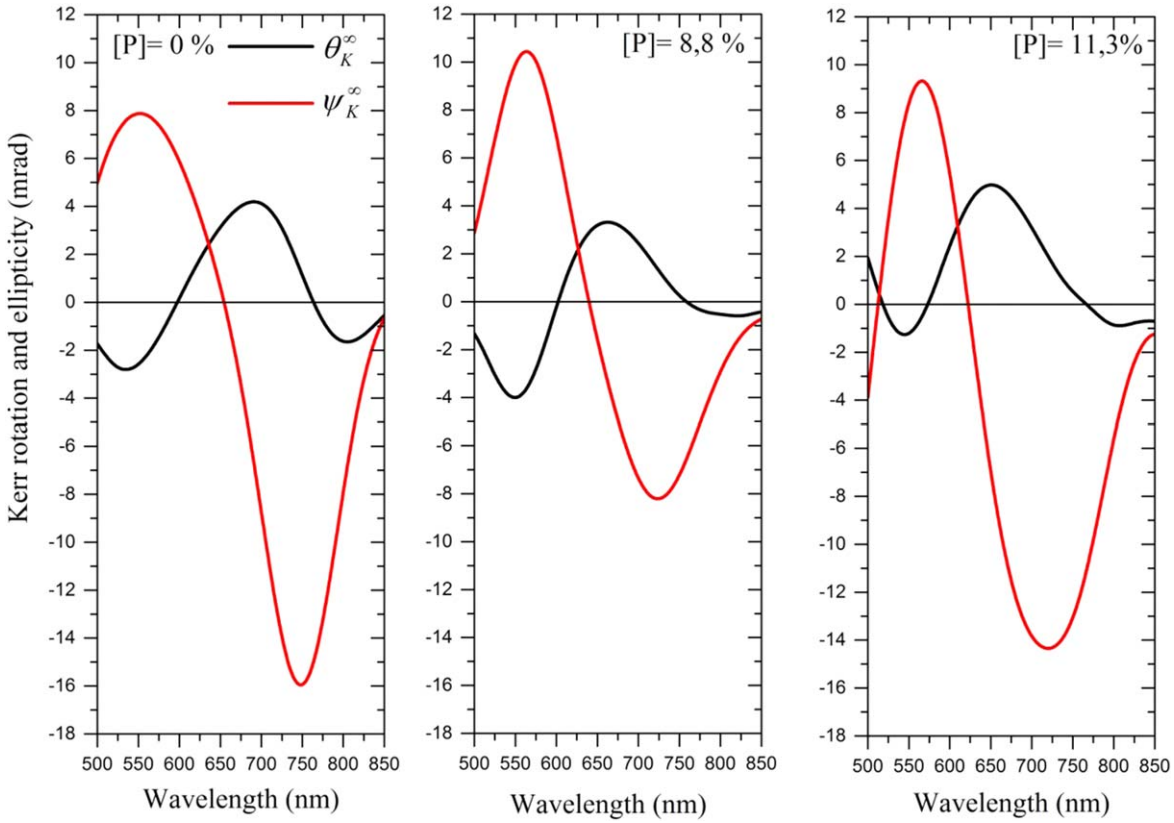

Figure 4. The functions $\theta_K^\infty(\lambda)$ and $\psi_K^\infty(\lambda)$ obtained from the experimental Kerr rotation and ellipticity and the wavelength dependence of the complex refractive index for samples A ([P] = 0%), B ([P] = 8.8%) and C ([P] = 11.3%). They represent the spectra expected for an infinite thickness.

observable, especially the enhancement of the ellipticity and the change of the shape of the Kerr rotation. In addition, the absolute value of ψ_K^∞ of A (B) layer decreases from 30 mrad (13 mrad) for d = 50 nm to 16 mrad (∼8 mrad) for d = $\pm\infty$. However, there is no significant spectral shift of the curves between the infinite and the actual thicknesses.

The Q_r and Q_i spectra for these samples are shown in figure 5. They were obtained from equations (3) and (4), after the determination of $\theta_K^\infty(\lambda)$ and $\psi_K^\infty(\lambda)$. Interestingly, the Q_r spectrum shows an extremum at the wavelength where Q_i tends to zero, at 750 nm, 723 nm and 714 nm for the concentrations [P] = 0%, [P] = 8.8% and [P] = 11.3%, respectively. The shape of Q_i and Q_r parts of the three layers reminds us of the expected behavior of the Kerr effect for a single oscillator optical transition [32]. One can notice that the Q_i and Q_r curves have a spectral behavior similar to the experimental Kerr rotation and ellipticity, respectively. With increasing phosphorus concentration, one can notes that the Q_i peak is shifted to the higher energies with increasing phosphorus concentration and its amplitude increases with respect to the Q_r one.

However, one can go one-step further and analyze the respective contributions of $Q_r(\lambda)$ and $Q_i(\lambda)$ in the experimental Kerr rotation and ellipticity spectra more in details. In figure 6 we plot the Kerr rotation and ellipticity spectra for sample A calculated using the real part Q_r obtained from the experimental spectra and the imaginary part Q_i set to zero (a) or the real part Q_r set to zero and the imaginary part Q_i obtained from the

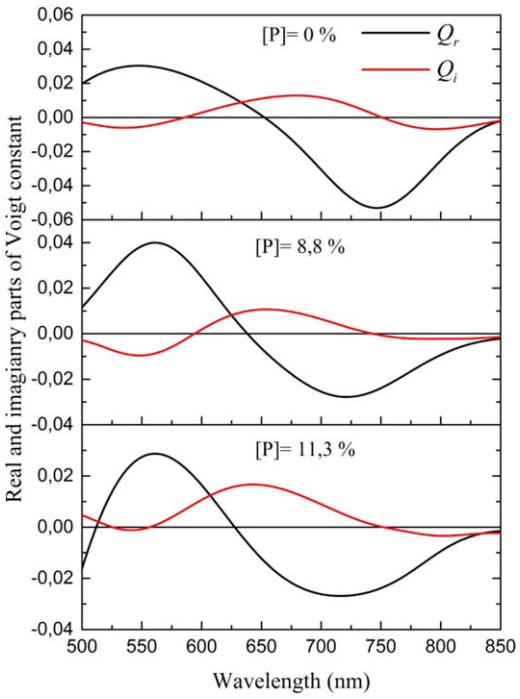

Figure 5. Real (Q_r) and imaginary (Q_i) parts of the magneto-optical Voigt constant of samples A (a), B (b) and C(c) as a function of the light wavelength. The wavelength dependence is extracted from the experimental Kerr rotation and ellipticity spectrum.

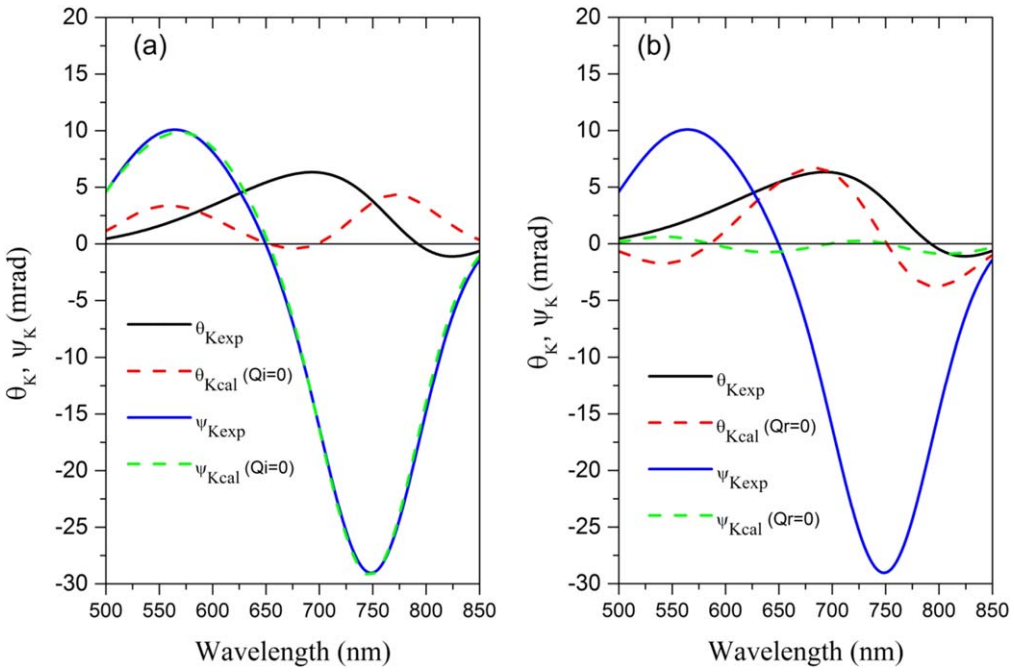

Figure 6. Contributions of the real and imaginary parts of the Voigt constant Q to the Kerr rotation and ellipticity for sample A. (a) Kerr rotation and ellipticity calculated with the real part Q_r obtained from the experimental spectra and the imaginary part Q_i set to zero (dashed line) compared the experimental spectra (full line). (b) Kerr rotation angle and ellipticity calculated with the real part Q_r set to zero and the imaginary part Q_i obtained from the experimental spectra (dashed line) compared the experimental spectra (full line).

experimental spectra (b). We compare the recalculated spectra to the experimental ones. Actually, the Q_r part alone can describe the Kerr ellipticity pretty well, which is not surprising since it appears in the form of the product $\eta\, Q_r$ which is dominant over the other terms ($\eta\, Q_i$, $\kappa\, Q_r$, $\kappa\, Q_i$). In contrast both $Q_r(\lambda)$ and $Q_i(\lambda)$ are necessary to describe properly the full Kerr rotation spectrum. However, if one is interested only in the maximum amplitude is well described by the Q_i term alone ($\eta\, Q_i$ term). As the dominant term in the ellipticity expression (equation (4)) is $\eta\ Q_r$, Terada *et al* proved this dependence and highlighted that the optical interferences, which are related to the phase shift in the materiel (essentially depends to the real part η), have an important influence on the Kerr ellipticity (also called magnetic circular dichroism in reflection configuration) shape in GaMnAs layer [24]. Also, via this model, we have shown that for full description of Kerr rotation the light absorption (described by κ Q_i term) in the materiel must be taken into account. Based on this model, future theoretical calculations could be developed and explain, with more details, the microscopic physical correlation between the Voigt constant and complex Kerr rotation.

In order to improve the sensitivity of TR-MOKE or Kerr microscopy [11, 39], it is crucial to optimize the Kerr signal for a fixed wavelength as a function of the layer thickness. By adopting the same model and referring to the equations (5) and (6), figure 7 shows the thickness dependence of the Kerr rotation and ellipticity of sample A for layer thicknesses up to 300 nm at a wavelength of 700 nm. The parameters used in this calculation are $\eta = 3.66$ and $\kappa = 0.23$ as obtained from the ellipsometric measurements at $\lambda = 700$ nm (extracted from figure 2). The Kerr coefficient is taken as $Q_r = -0.0306 \pm 410^{-4}$ and $Q_i = 0.012 \pm 2\ 10^{-3}$ (obtained experimentally from figure 5). Using

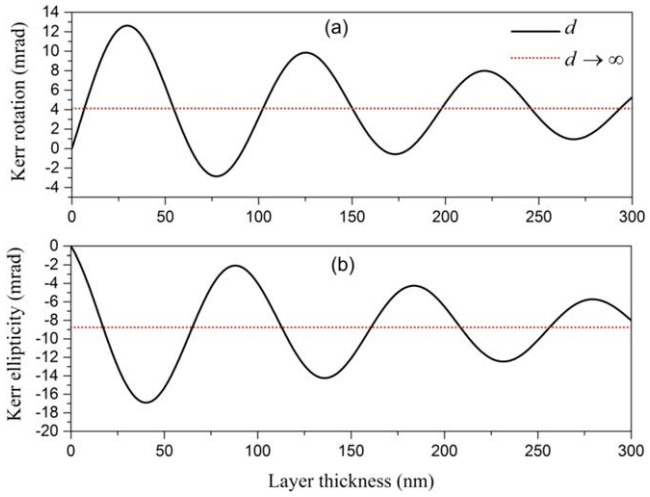

Figure 7. Dependence of Kerr rotation (a) and ellipticity (b) on the layer thickness of sample A. The red dashed line represents the Kerr rotation and ellipticity for a layer of infinite thickness.

the same parameters at $\lambda = 700$ nm, the values of Kerr rotation and Kerr ellipticity for infinite thicknesses (for $d \to \infty$) were extracted from the two equations (3) and (4). One can see for example that the Kerr rotation is enhanced for $d = (2p + 1)\ \lambda/8\eta$ and takes the $d \to \infty$ value for $d = p\lambda/4\eta$, where p is an integer. For $\lambda = 700$ nm the wavelength of light in the material is $\lambda/\eta \approx 190$ nm. A thickness of 50 nm ($\approx\lambda/4\eta$) as that of our samples is not appropriate to enhance the Kerr rotation. Thicknesses around 25 nm or 75 nm would have been more appropriate. Also, one can notice that the Kerr ellipticity is stronger than the Kerr rotation. It can be more interesting to use in

TR-MOKE studies. In this case, the change in the optimum thickness must be taken into account.

5. Conclusion

The spectral variation of the Kerr rotation and Kerr ellipticity for three films with different phosphorus doping was measured by magneto-optical polar Kerr effect. Using an optical layer model which takes into account the experimental PMOKE spectra and the spectral dependence of the complex refractive index of the layer, the intrinsic magneto-optical Voigt constant Q, which describes the influence of the magnetization on the off-diagonal elements of the dielectric permittivity tensor, was determined for the three layers in the spectral range between 500 nm and 850 nm. By exploiting the spectral dependence of the real and imaginary parts of Q, we can identify the contribution of each part on the Kerr rotation and ellipticity. We found that the Kerr ellipticity evolution could be described by the imaginary part (Q_i) alone while in order to account properly for the shape of the Kerr rotation both the real and imaginary parts of the Voigt constant are necessary. For a fixed wavelength at 700 nm, the variation of θ_K and ψ_K as a function a layer thickness is determined for GaMnAs layer. This study allows optimizing the optical detection of Kerr microscopy or TR-MOKE measurements.

Acknowledgments

H Riahi would like to thank Dr Khaled Ben Saad from the Centre de Recherches et de Technologies de l'Energie (CRTEn)-Borj Cédria-Tunisie, for his assistance with the spectral Kerr setup and Dr Bruno Gallas for his ellipsometry measurements. He acknowledges insightful advices from Dr C Gourdon and Dr L Thevenard from Institut des Nanosciences de Paris, France.

ORCID iDs

H Riahi https://orcid.org/0000-0002-7889-7941
A Lemaître https://orcid.org/0000-0003-1892-9726

References

[1] Hubert A and Schäfer R 2000 *Magnetic Domains* (Berlin: Springer)
[2] Zvezdin A K and Kotov V A 1997 *Modern Magneto-optics and Magneto-optical Materials* (New York: Taylor and Francis Group)
[3] Mansuripur M 1995 *The Physical Principles of Magneto-optical Recording* (Cambridge: Cambridge University Press)
[4] Parkin S S P, Hayashi M and Thomas L 2008 *Science* **320** 190–4
[5] Dourlat A, Jeudy V, Lemaître A and Gourdon C 2008 *Phys. Rev.* B **78** 161303
[6] Haghgoo S, Cubukcu M, von Bardeleben H J, Thevenard L, Lemaître A and Gourdon C 2010 *Phys. Rev.* B **82** 041301
[7] Wang K Y, Irvine A C, Wunderlich J, Edmonds K W, Rushforth A W, Campion R P, Foxon C T, Williams D A and Gallagher B L 2008 *New J. Phys.* **10** 085007
[8] Yamanouchi M, Chiba D, Matsukura F, Dietl T and Ohno H 2006 *Phys. Rev. Lett.* **96** 096601
[9] Wang K Y *et al* 2010 *Appl. Phys. Lett.* **97** 262102
[10] Shihab S, Riahi H, Thevenard L, von Bardeleben H J, Lemaître A and Gourdon C 2015 *Appl. Phys. Lett.* **106** 142408
[11] Němec P *et al* 2013 *Nat. Com* **4** 1422
[12] Němec P *et al* 2013 *Nat. Phot* **7** 492–8
[13] Chernyshov A, Overby M, Liu X, Furdyna J K, Lyanda-Geller Y and Rokhinson L P 2009 *Nat. Phys.* **5** 656–9
[14] Li Y *et al* 2013 *Appl. Phys. Lett.* **103** 022401
[15] Thevenard L, Duquesne J-Y, Peronne E, von Bardeleben H J, Jaffres H, Ruttala S, George J-M, Lemaître A and Gourdon C 2013 *Phys. Rev.* B **87** 144402
[16] Thevenard L, Camara I S, Prieur J-Y, Rovillain P, Lemaître A, Gourdon C and Duquesne J-Y 2016 *Phys. Rev.* B **93** 140405
[17] Lemaître A, Miard A, Travers L, Mauguin O, Largeau L, Gourdon C, Jeudy V, Tran M and George J-M 2008 *Appl. Phys. Lett.* **93** 021123
[18] Zemen J, Kučera J, Olejník K and Jungwirth T 2009 *Phys. Rev.* B **80** 155203
[19] Dietl T and Ohno H 2014 *Rev. Mod. Phys.* **86** 187
[20] Thevenard L, Gourdon C, Haghgoo S, Adam J-P, von Bardeleben H J, Lemaître A, Schoch W and Thiaville A 2011 *Phys. Rev.* B **83** 245211
[21] Hamrle J, Pištora J, Hillebrands B, Lenk B and Münzenberg M 2010 *J. Phys. D: Appl. Phys.* **43** 325004
[22] Shihab S, Thevenard L, Lemaître A and Gourdon C 2017 *Phys. Rev.* B **95** 144411
[23] Sun C, Kono J, Cho Y-H, Wócik A K, Belyanin A and Munekata H 2011 *Phys. Rev.* B **83** 125206
[24] Terada H, Ohya S and Tanaka M 2015 *Appl. Phys. Lett.* **106** 222406
[25] Du Trémolet de Lacheisserie E, Gignoux D and Schlenker M 2005 *Magnetism: Fundamentals* (New York: Springer Science & Business Media) p 405
[26] Zak J, Moog E R, Liu C and Bader S D 1991 *Phys. Rev.* B **43** 6423
[27] Haidu F, Fronk M, Gordan O D, Scarlat C, Salvan G and Zhan D R T 2011 *Phys. Rev.* B **84** 195203
[28] Liu H L, Lu K S, Kuo M X, Uba L, Uba S, Wang L M and Jeng H-T 2006 *J. Appl. Phys.* **99** 043908
[29] Cubukcu M, Bardeleben H J V, Khazen K, Cantin J L, Manguin O, Largeau L and Lemâitre A 2010 *Phys. Rev.* B **81** 041202
[30] Casiraghi A *et al* 2010 *Appl. Phys. Lett.* **97** 122504
[31] Riahi H, Thevenard L, Maaref M A, Gallas B, Lemaître A and Gourdon C 2015 *J. Magn. Magn. Mater.* **395** 340–4
[32] Yahyaoui M, Riahi H, Maaref M A, Boujdaria K, Lemaître A, Thevenard L and Gourdon C 2017 *J. Appl. Phys.* **121** 125702
[33] Sato K 1981 *J. Appl. Phys.* **20** 2403–9
[34] Neffati R, Saïdi I and Boujdaria K 2012 *J. Appl. Phys.* **112** 053716
[35] Rosa P, Sangalli D, Onida G and Debernardi A 2015 *Phys. Rev.* B **91** 075207
[36] Tesařová N *et al* 2014 *Phy. Rev.* B **89** 085203
[37] Yahyaoui M, Boujdaria K, Cubukcu M, Testelin C and Gourdon G 2013 *J. Phys. Condens. Matt* **25** 429501
[38] Rui Qiang Z, Kui Juan J, HaiZhong G, HuiBin L and GuoZhen Y 2013 *Sci. China-Phys. Mech. Astro* **56** 2370–6
[39] Tesařová N *et al* 2014 *Phys. Rev.* B **90** 15520